

## TWO-DIMENSIONAL KINEMATIC FAULT MODELING OF THE PACOIMA DAM STRONG-MOTION RECORDINGS OF THE FEBRUARY 9, 1971, SAN FERNANDO EARTHQUAKE

BY DAVID M. BOORE AND MARK D. ZOBACK

### ABSTRACT

A simple, uncontrived model of the rupture during the San Fernando earthquake can explain the main features of the particle velocity traces derived from the accelerograms recorded at Pacoima Dam. This result, combined with the probable small effect of surface topography on the velocity traces, strengthens the case for acceptance of the peak particle velocity at Pacoima Dam (115 cm/sec) as a valid ground-motion parameter for design purposes in earthquake engineering.

Most of the conspicuous motion on the velocity traces during the first 4 sec after triggering seems to result from thrust faulting, starting at a focal depth within several kilometers of 14 km, on a fault surface dipping at least  $50^\circ$  and extending only part way to the surface at a velocity near 2.5 km/sec. The data also indicate that this faulting continued to the surface at a slower rupture velocity (less than 2 km/sec) along a less steeply dipping surface.

The amount of relative offset across the fault surface is difficult to determine, both because of inherent limitations in the two-dimensional model and because of nonuniqueness in the fitting of the data. The estimates of this dislocation, however, are consistent with the wide range of values reported by other authors in studies using various types of data. The data are also consistent with a model suggested by Alewine and Jordan (1973) and Trifunac (1974) in which the total dislocation has a minimum near the center of the fault surface, with approximately equal amounts of total offset on the fault near the hypocenter and near the Earth's surface.

### INTRODUCTION

The Pacoima Dam strong-motion recordings of the San Fernando earthquake, February 9, 1971, are important for at least two reasons. First, they represent the strongest ground shaking yet recorded from an earthquake (Trifunac and Hudson, 1971) and second, they offer a rare opportunity to investigate the rupture mechanism of an earthquake from near-field measurements. The records are especially significant in the field of engineering seismology, where earthquake motions used in building design must often be based upon the extrapolation of motions recorded at relatively great distances.

Because of their importance, the Pacoima Dam recordings have received attention from growing numbers of investigators. There has been speculation that the recordings are strongly influenced by local site effects and, thus, should not be used for design purposes. Attempts to explain the records by models of the earthquake can aid in deciding to what extent the records are anomalous. Bolt (1972) and Hanks (1974) applied ray-theory arguments to show that several features occurring during the first few seconds of record-

ing could be explained in terms of a simple model of faulting. Hanks' detailed study suggested that the predominate motion during the first several seconds was associated with a large dislocation and stress drop on a small region of the fault near the hypocenter. Simulations of the wave forms have been made by several investigators (Tsai and Patton, 1972; Mikumo, 1973; and Trifunac, 1974; among others) using various dislocation models. Although they differ in detail, most of the studies find that relatively simple models can reproduce in a gross way the first few seconds of motion.

Our study emphasizes the sensitivity of the recorded motion to many of the parameters involved and points out the ambiguities in the interpretations if some of these parameters cannot be estimated independently. In spite of these ambiguities, we think it significant that a very simplified model can explain the major features of the recorded motion. In particular, in contrast to the peak acceleration, the large pulse in the particle velocity is clearly associated with the initial rupture. This, combined with the relatively small effect of surface topography on the velocity wave form (Boore, 1973), makes it easier to accept the peak particle velocity as a valid point upon which to base design motions for various engineering projects.

We use a two-dimensional dislocation model of the fault to synthesize wave forms. The technique, assumptions, and limitations are fully described by Boore and Zoback (1974).

The paper begins with a general description of the faulting process. After this, we discuss the acceleration data and the particle velocities obtained from it. Estimates of the focal depth are then made from the time difference between the *S* and *P* waves from the hypocenter. Following this, the main section of the paper describes the inferences we can make about the rupture process from attempts at matching observed and theoretical particle-velocity wave forms. The final section discusses some of the ambiguity in the inferred rupture parameters and compares our findings with those from other studies.

#### GENERAL DESCRIPTION OF FAULTING

Any model for the earthquake should be generally consistent with results inferred from other data. Results of other studies of the San Fernando earthquake can be summarized briefly. The epicentral location of the earthquake as determined by Allen *et al.* (1973) from body-wave data is shown in Figure 1. Focal-depth determinations range from 8 to 13 km, with an uncertainty of at least 5 km (Allen *et al.*, 1971; Allen *et al.*, 1973). Fault-plane solutions (for example, Dillinger and Espinosa, 1971; Wesson *et al.*, 1971; Whitcomb, 1971) show the motion near the hypocenter to be predominantly thrust on a plane dipping approximately 50°. Surface measurements indicate approximately equal amounts of left-lateral strike-slip and thrust motion, with a net dislocation of approximately 2 m on a plane dipping less steeply than indicated by the fault-plane solutions (Kamb *et al.*, 1971). Aftershock locations (Figure 1) outline a roughly triangular shaped region.

These studies suggest that a simplified model of the earthquake would have the initial rupture start around 10 km as predominantly thrust motion on a fault plane with about 50° dip and then spread upward and laterally on a plane that decreased in dip toward the surface. As the rupture approached the surface, the strike-slip component would eventually become as large as the thrust component of motion. We have found a model, consistent with this general description of the earthquake, that reproduces the main features of the first few seconds of the particle velocity traces.

## DATA

*Acceleration.* The accelerations recorded on the left abutment of Pacoima Dam during the earthquake are shown in Figure 2. The time scale is referenced to the triggering of the instrument, which was probably caused by the initial *P* waves from the

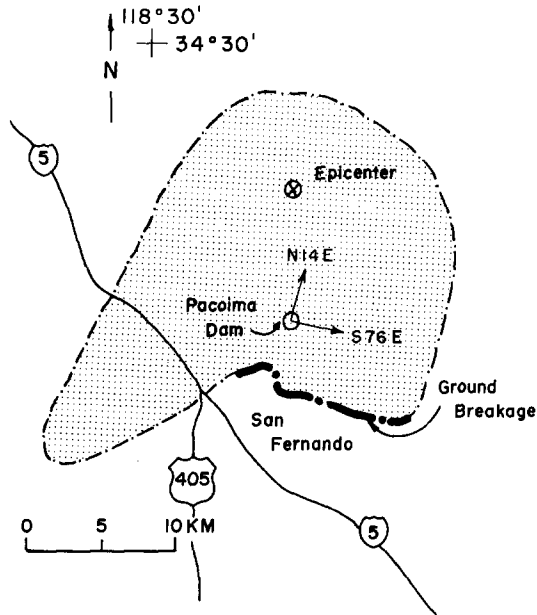


FIG. 1. Map of area near San Fernando, California, showing the earthquake epicenter, aftershock zone (stippled), and ground breakage associated with the earthquake of February 9, 1971. Arrows at Pacoima Dam show directions of strong-motion recording.

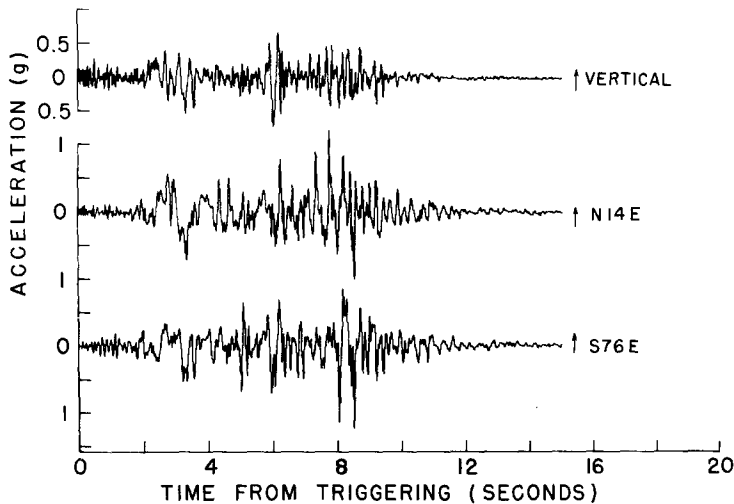


FIG. 2. Accelerograms recorded at Pacoima Dam.

hypocenter (Trifunac and Hudson, 1971). The records show considerable character, both in amplitude and frequency content. The largest accelerations, in excess of 1 *g*, occur around 8.0 sec. These later motions are difficult to explain by a simple, smoothly propagating fault. On the other hand, the longer-period motions around 2.0 to 4.0 sec are clearly related to the faulting process. Between these two features, several other

coherent phases are present. Positive identification of these phases could be an important constraint on the later part of the rupture process.

Particle-motion diagrams were constructed from the horizontal components of the accelerograms for consecutive time windows (Figure 3). The direction to the epicenter and the directions into which the velocity traces were rotated are shown for reference (see Figure 4). Although not rectilinear, the particle motions show a definite trend. This is true not only for the section that is most easily explained by simple rupture models

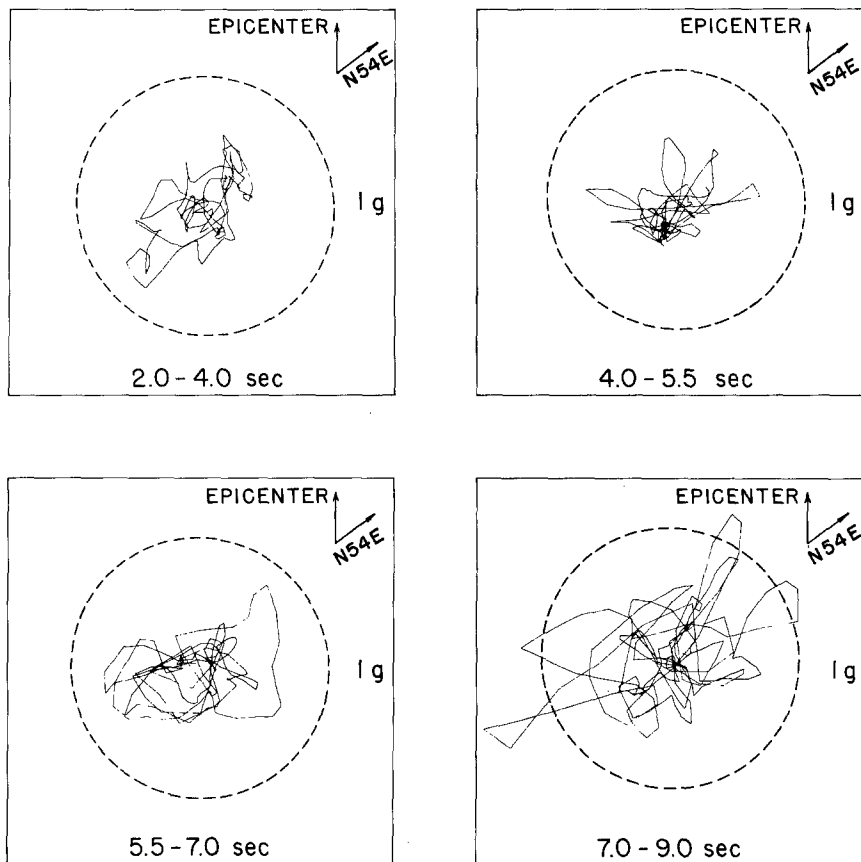


FIG. 3. Particle motion plots of horizontal accelerations. Direction of epicenter and direction of rotation of the velocity traces are included for reference, as is the circle of 1- $g$  acceleration. The same scale is used in all time windows.

(2.0–4.0 sec) but also for the section in which the peak accelerations are found (7.0–9.0 sec; note that the peak vectorial acceleration is 1.5  $g$ ). The motions in this latter time period are commonly explained as random radiation from small sections of the fault (Bolt, 1972). The consistent directions of particle motion should serve as a constraint on the locations on the fault plane from which these motions could originate. We have not pursued this point here. Such a study would use the vertical motion in an attempt to separate  $SV$  and  $SH$  motion. Then, with the assumption that the acceleration peaks are radiated from parts of the fault that can be treated as point sources, the particle-motion diagrams in Figure 3 could be used to define sectors of the fault from which radiation occurred. Implicit in such an analysis would be the assumption that near-surface effects, such as topography, will not change the polarization characteristics of the incoming waves. Topography probably does influence the amplitudes of the accelerations

(Boore, 1973), especially in the later part of the record, but the consistent trend shown for the data in most of the time windows in Figure 3 suggests that the polarization is not influenced by the topography.

*Velocity.* Straightforward integration of the accelerograms produced the particle velocity traces in the upper part of Figure 4. We have chosen as a compromise to use velocity as the data against which models of the faulting are tested. The acceleration traces contain more information, but they are too sensitive to minor details of faulting,

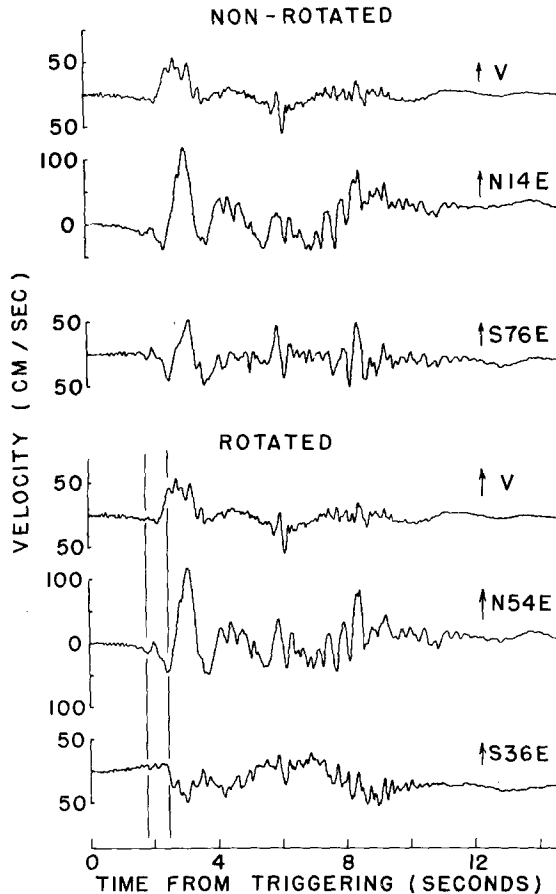


FIG. 4. Particle velocities obtained by integrating the accelerograms. Vertical lines in rotated traces show possible picks of the *S* arrival.

geological heterogeneities, and surface topography. Displacement traces, on the other hand, do not show as much character as do the velocity traces and also have considerable motion in the time window during which surface waves should arrive (our model is incapable of predicting the surface-wave motion). Furthermore, current ideas of source mechanics (Brune, 1970) suggest that in the near-field particle velocity amplitude scales directly with the stress available to drive the fault. Thus, particle velocity is a more fundamental parameter than displacement or acceleration.

For modeling purposes, it is desirable to rotate the horizontal particle velocities into a coordinate system which separates the motion due to the strike-slip and the thrust components of faulting. The fault-plane solutions show a strike of close to  $N60^{\circ}W$ ; the horizontal projection of the thrust component of faulting should, thus, be in the  $N30^{\circ}E$  direction (Dillinger and Espinosa, 1971). Figure 4 shows the particle velocity in

coordinate systems which bracket this value. The horizontal components close to the thrust direction (the middle trace in the *upper* and *lower* parts of Figure 4) show little sensitivity to the rotation. The strike-slip component, however, changes character with rotation and shows the least amount of correlation with the thrust component, in the time window 2.0–4.0 sec, when an assumed strike of the fault of about N40°W to N50°W is used in the rotation (this can also be seen in Figure 3). Regardless of the angle to be used in the rotation, the results suggest that the strike-slip component during the first few seconds of rupture is not as important as the thrust motion. This conclusion agrees with the inferences from the fault-plane solutions. In this paper, the strike-slip motion is ignored; the vertical and horizontal components are hereafter designated  $V$  and  $H$ .

The characteristics of the particle motions that were most emphasized in the wave-form modeling were the shapes and relative amplitudes of the pulses occurring between 2 and 4 sec. The relative amplitudes, as measured by the  $H/V$  ratio ( $\simeq 2.3$  for the data), were particularly useful in the modeling; several otherwise reasonable models could be rejected because their  $H/V$  ratio was less than or only slightly larger than unity.

#### FOCAL DEPTH

Identification of direct  $P$  and  $S$  waves from the hypocenter gives a  $t_s - t_p$  time difference that can be used to estimate the hypocentral distance and, in combination with an epicentral determination from the permanent network of standard seismometers, the focal depth of the earthquake. It is evident from the records (Figure 4) that a low-level long-period phase begins at 1.7 sec after triggering. Bolt (1972) identifies this as  $S$ . The models in this paper, however, show that  $S$  should begin as a sharp upswing (in the coordinates used in Figure 4). The most dominant phase on the record has this characteristic; the phase arrives on the horizontal component at 2.4 sec and has been assumed by Hanks (1974) to correspond to the  $S$  wave from the hypocenter. On the other hand, the obvious upswing on the vertical component occurs between 1.7 and 2.4 sec. Thus, the choice of the initial  $S$  wave is somewhat uncertain. This probably indicates that the faulting is not as simple as assumed in our model, although the predictions of our model agree with the major features of the data. For this reason, we prefer to identify the arrival at 2.4 sec after triggering as the  $S$  wave from the hypocenter. We also assume that the strong-motion instrument was triggered by the initial  $P$  wave from the hypocenter.

The choice of the  $t_s - t_p$  interval will affect the estimate of focal depth. To see the uncertainty, we computed  $t_s - t_p$  times for two assumed depths, 8.5 and 14 km, using a range of  $P$  and  $S$  velocities under the assumption that the relative location of Pacoima Dam and the epicenter are correct as shown in Figure 1. In Figure 5,  $t_s - t_p$  is plotted against  $\sigma$ , the Poisson's ratio, with the  $P$  velocity as a parameter. The average  $P$  velocity of the crystalline rocks probably lies within the 5.0 to 6.0 km/sec band. If we accept 1.7 sec as the  $t_s - t_p$  time, a depth near 8.5 km corresponds to reasonable values of Poisson's ratio (0.23 to 0.29). On the other hand,  $t_s - t_p = 2.4$  sec leads to a depth close to 13 or 14 km. This is consistent with  $pP$  analysis of Hanks (1974) and spectral analysis of surface waves (Canitez and Toksöz, 1972) and is within the uncertainty in the hypocenter location of Allen *et al.* (1973). We have accepted 2.4 sec as the  $t_s - t_p$  time and adopted a focal depth of 14 km in most of our simulations. The simulated wave forms do not change significantly for focal depth within several kilometers of 14 km.

In the analysis above, we assumed an epicentral distance and determined the depth. The required Poisson's ratio was close to 0.29 for  $P$  velocities between 5.5 and 6.0 km/sec. If a Poisson's ratio of 0.25 is assumed, then either the epicentral distance or focal depth must be increased. The value of Poisson's ratio in crystalline rocks can vary from less than

0.25 to greater than 0.30 (Birch, 1966; Christensen, 1966). Because of this uncertainty, we feel the value near 0.29 indicated from Figure 5 is reasonable. If a value of 0.25 were used, the increase in hypocentral distance would be only a few kilometers.

### SIMULATIONS

The method used to calculate the theoretical wave forms has been discussed in detail by Boore and Zoback (1974). As explained there, the method has several limitations and, thus, a conscious effort must be made not to exceed the inherent limitations of the method in trying to match the data with the theoretical wave forms. If we included enough

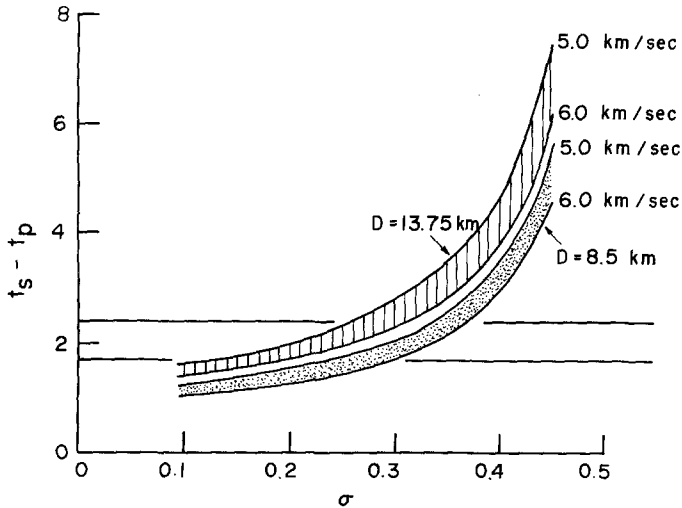


FIG. 5. Time difference between  $S$  and  $P$  arrivals as a function of focal depth  $D$ ,  $P$  velocity, and Poisson's ratio ( $\sigma$ ). Horizontal lines are possible  $t_s - t_p$  times shown in previous figure. Shaded areas represent choices of  $P$  velocity between 5.0 and 6.0 km/sec.

parameters in our model, we could fit the data almost perfectly, but the resulting model would have little meaning. We have attempted to use simple uncontrived models that are consistent with other information. The wave forms for several different models are discussed in order to illustrate some of these constraints and to provide insight into the importance of some of the parameters. At the risk of confusion, one figure may contain the information needed for several types of comparisons.

Several parameters are available to model the faulting process: geometry of the fault plane, dislocation variation in time, rise time, total dislocation, rupture velocity, and material velocities. Several fault segments can be used, with independent choice of all of the parameters above except the  $P$  and  $S$  velocity. In all of the examples that follow, the  $P$  and  $S$  velocities are 5.7 and 3.1 km/sec. These could be changed, without appreciably affecting the results, as long as both the  $t_s - t_p$  time and the ratio of rupture and shear velocity are constant. Two dislocation functions have been used, a truncated ramp and a rounded ramp (shown in Figure 6 with a rise time of 1 sec). The rise time used in the models is 0.6 sec. This was determined after several model runs and gives the best fit to the data, holding the other parameters fixed.

To facilitate scaling of the theoretical wave forms to the data, a total dislocation of 1 m was used in the models. In the figures, the  $H$  and  $V$  traces for a given model are plotted with the proper relative amplitude. The wave forms for different models are not plotted

to the same scale. Comparisons between models can be made by using the peak velocity (noted in m/sec) shown for each wave form.

Our initial efforts involved models with focal depths given by the main shock hypocenter location. The left side of Figure 7 shows a schematic profile of such a model that is consistent with the hypocenter of Allen *et al.* (1973) and the observed ground breakage. The wave forms show the prominent *S* arrival beginning as an upswing, but the relative amplitudes of the vertical (*V*) and horizontal (*H*) traces are not consistent with the data. The model on the right has a greater focal depth (14 km) and a dip of 52°. If rupture continues to the surface on this fault, it would produce the motions given by solid lines.

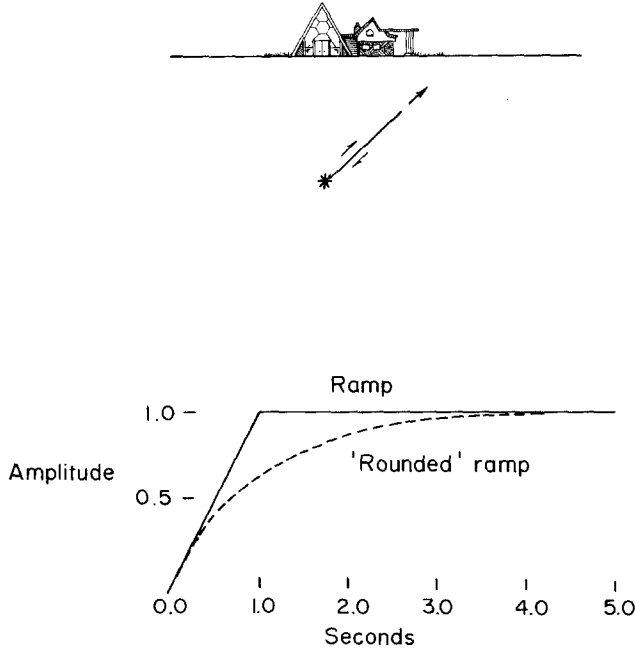


FIG. 6. *Top*, schematic profile of fault: it starts at depth and propagates upward at a constant rupture velocity. *Bottom*, the two dislocation time functions considered in the text are shown here with a rise time of 1.0 sec.

The  $H/V$  ratio for these wave forms is larger than given by the model on the left of the figure, but again the match with the data is not very good. If, however, the fault propagation is stopped at depth (at a point shown by the bar approximately halfway along the fault plane) the wave forms, shown by the dashed curves, are more consistent with the data. Not allowing the rupture to propagate to the surface on the plane dipping at 52° is consistent with the lack of major surface fracturing along the predicted line of intersection. Although a small segment of the fault east of the Veterans Hospital seems to have a tectonic origin (Kamb *et al.*, 1971 and U.S. Geological Survey Staff, 1971), most of the observed surface rupture occurs farther south, and this, combined with after-shock locations, suggests a decrease in the fault dip as the surface is approached. As shown later, including an upper segment of less steeply dipping fault surface does not greatly change the wave form characteristics produced by the partial fault in Figure 7.

Figure 7 also shows the effect of rupture velocity and the lack of a dominant phase associated with the passage of the rupture front beneath the station. As discussed in Boore and Zoback (1974), the ratio of the rupture to the shear velocity (the Mach number)

is an important variable in the simulations. An increase in the Mach number produces an increase in the peak amplitude of the motion and a decrease in its width.

The time denoted by  $R_s$  in the figures is the predicted arrival time of a hypothetical phase that travels at the rupture velocity to the point on the fault closest to the station, and then at the  $S$  velocity to the station. Bolt (1972) assumed the existence of such a phase to infer the rupture velocity during the San Fernando earthquake. Contrary to our initial expectations, no distinct motion arrives at the time indicated for this phase.

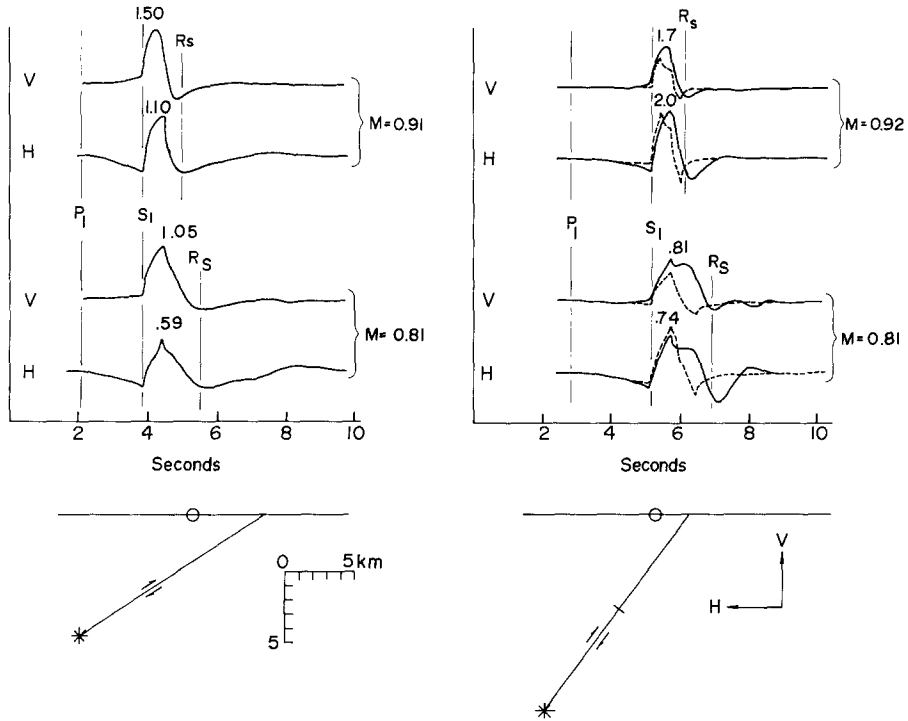


FIG. 7. Theoretical velocity wave forms for the models sketched at the bottom. The recording location, shown by the circle, and epicenter are consistent with those shown in Figure 1. The time scale is referenced to the origin time; the  $P$  and  $S$  waves from the hypocenter are denoted  $P_1$  and  $S_1$ .  $M$  is the Mach number. The dashed curves on the right are produced by a fault that stops at the crossbar about halfway up the fault plane. The dashed and solid curves are not drawn to the same scale; the numbers refer to the solid lines and give the peak velocity in meters per second produced by a ramp dislocation on the fault with 0.6-sec rise time and 1-m total displacement. For comparison, amplitudes of the horizontal component from the buried fault (dashed line) are 1.86 and 1.03 m/sec for Mach numbers of 0.92 and 0.81, respectively.

The motion that Bolt identified as  $R_s$  on the record occurs between the  $S$  and  $R_s$  arrival times.

The  $H/V$  ratio depends not only on dip of the fault but also on the location of the station with respect to the fault. For the partial fault dipping at  $52^\circ$ , the  $H/V$  ratio is greater than unity if the station is located to the north of the surface projection of the fault plane (Figure 8). The dependence of the  $H/V$  ratio on the relative locations of the surface projection and the station argues against either a shallower focal depth or an epicenter farther north, as proposed by Hanks (1974). In either situation, the effect would be to move the Pacoima Dam site from point A to point B, thus making it more difficult to explain the  $H/V$  ratio. On the other hand, the  $H/V$  ratio can be made larger by increasing the dip of the fault or by allowing for the upward refraction of rays as they propagate into lower velocity materials near the surface (from simple Snell's law arguments, the

ratio could be increased by about 50 per cent if the velocity at the surface were 0.8 that at depths of 10 or 14 km). Both effects would counteract the dependence of the  $H/V$  ratio on the relative location of the station and surface projection of the fault and would allow for an epicenter farther north. The  $H/V$  ratio from the model, however, is smaller than the measured ratio (1.7 versus 2.3), and the effect of a decreasing velocity or an increasing fault dip would help bring the model results into accord with the measured results without moving the epicenter to the north. Thus, a complicated trade-off may exist between all of these effects; the main conclusions of this paper are not influenced by uncertainties of 3 km or so in the epicenter location.

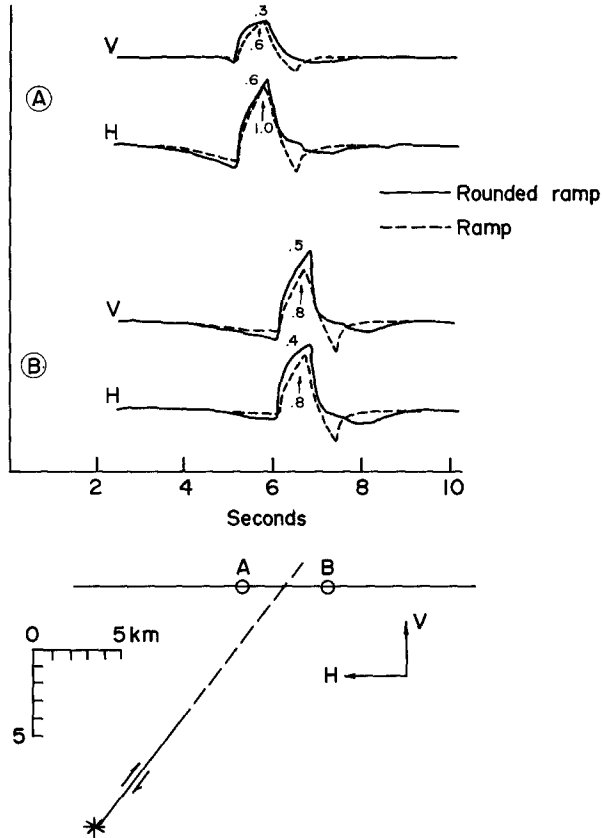


FIG. 8. Comparison of wave forms on either side of the surface projection of a fault that stops at depth. Wave forms for both ramp and rounded ramp are shown. The dashed and solid curves are not drawn to the same scale.

Figure 8 also contains a comparison of the wave forms produced by the two dislocation functions discussed earlier. The difference in wave shape is not great. The rounded ramp produces a larger  $H/V$  ratio, but the ramp dislocation function produces a wave form that resembles the data somewhat better, especially in the later part of the large pulse. The ramp dislocation function has been used in all of the figures except for Figure 8.

The comparison between the data and the theoretical wave form for the model that starts at 14 km with a dip of  $52^\circ$  and propagates part way to the surface at a velocity of 2.5 km/sec is shown at the top of Figure 9. Although we consider the fit to be quite good, especially in view of the simplicity of the model, it could probably be improved by

making adjustments of the many available parameters. We believe the major features of the record have been duplicated by this model.

It is obvious that the faulting did not stop at depth but came to the surface. We have modeled this by adding another dislocation to the first (Figure 9, *bottom*). In this example we have assigned a slower rupture velocity (1.86 km/sec) to this upper segment in an attempt to produce the long-period undulatory motion that follows the main pulse. The wave forms produced when both dislocations have the same amplitudes and the upper dislocation begins at the time of arrival of the rupture on the lower dislocation are shown

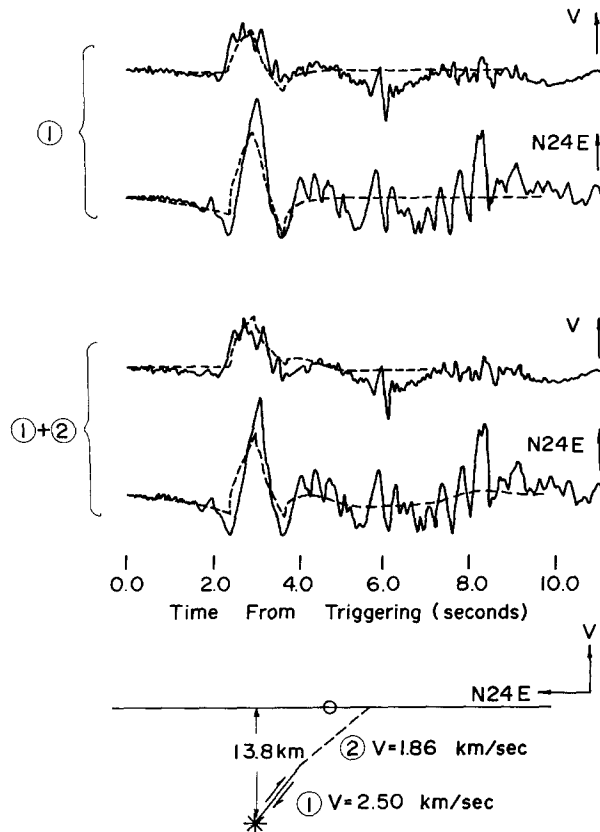


FIG. 9. Comparison of theoretical wave forms and data. (1) represents the lower segment of faulting and (2) represents the upper segment. The two *top* traces include only the contribution from (1), whereas the *lower* traces include the contributions from (1) and (2). A ramp dislocation function with 0.6-sec rise time was used.

at the bottom of Figure 9. As expected, some of the long-period motion can be reproduced, but surface-wave contributions, which are not produced by our model, are also expected to arrive during this time period. For this reason, we have not made a serious attempt to match this part of the data. If the rupture velocities for the two dislocations in Figure 9 are correct, *S* waves from the breakout of the fault at the surface will arrive approximately 8 sec after the triggering of the instrument. The largest accelerations in the data occur near this time (Figure 2). The clear phase near 5.5 sec (best seen in Figure 4) is not explained by our simple model. If it is associated with the breakout, rupture velocities close to 3 km/sec would be required. If this were true, the long-period motions following the large velocity pulse could not be produced by the rupture process as we have modeled it. It is more likely that this phase is due to an "aftershock" of the main

event produced by a slowing of the rupture at some point at depth. In this sense, it is similar to the multiple rupture proposed by previous authors for other earthquakes (Wyss and Brune, 1967; Trifunac and Brune, 1970).

The  $H/V$  amplitude ratio for the wave motion from the combined faults in the lower part of Figure 9 is smaller than it was for the single fault at depth. Figure 10 shows the contributions from fault segments (1) and (2) before adding. By visually shifting the second trace, it can be seen that, regardless of when the rupture on the upper fault is initiated (within reason), the motion from the second fault will decrease the  $H/V$  ratio. Using higher rupture velocities on the upper segment does not improve this situation. It might be possible both to preserve the  $H/V$  relation and to produce the later long-period motions by assigning a small amount of slip on the first part of the upper dislocation. This would reduce the amplitude of the motion that is responsible for decreasing the  $H/V$  ratio. The slip distribution with distance along the fault plane would then be

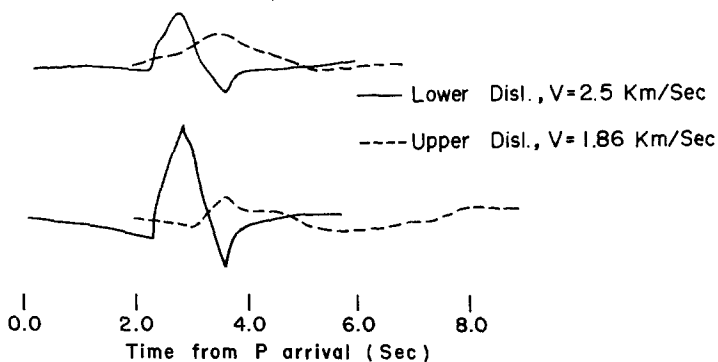


FIG. 10. Separate contribution from fault segments (1) and (2) in Figure 9. Relative amplitudes of traces are correct; identical dislocation functions on both fault segments were used in the calculations.

qualitatively similar to that proposed by Alewine and Jordan (1973) and Trifunac (1974)—high at bottom and top with a minimum near the center of the fault surface. The results for such a model are shown in Figure 11, in which the relative amplitude of the dislocation on the first part of the upper dislocation has been reduced from 1.0 to 0.5. As expected, the  $H/V$  ratio has been increased without changing the longer-period motions (compare with Figure 9, bottom). These results are only speculative; further attempts at matching the long-period motions have not been undertaken because of the possible presence of surface waves in the data.

#### DISCUSSION

Comparisons of theoretical wave forms and the recorded data in the section above helped put constraints on the geometry of the faulting and showed that a simple fault model could explain the prominent features of the particle velocity records. It should also be possible to estimate the amount of slip on the fault plane by scaling the calculated motion to the data. This, however, is difficult to do with any precision for two reasons. First, the method used in the calculations is based on a two-dimensional idealization of the fault. The dependence of amplitude on distance from the fault is different than for the three-dimensional model, although the wave forms are similar (Boore and Zoback, 1974). Second, the inferred slip distribution is uncertain because different models produce wave forms of similar shape but different amplitude.

Examples of the inconclusive fit of the models and the associated uncertainty in slip on the fault are shown in several figures. For example, the ramp and rounded ramp dislocation functions with 1m total dislocation used for the upper part of Figure 8 produce

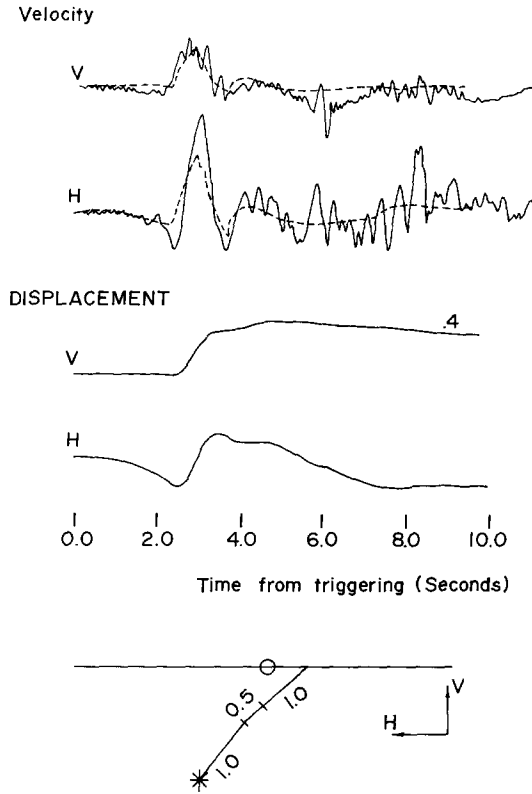


FIG. 11. Velocity (dashed lines) and displacement for a model in which the total dislocation has a minimum midway along the rupture surface. The static vertical displacement produced by the dislocations shown is 0.4 m. The displacement trace has not been high-pass filtered, and, thus, comparisons with the displacement traces calculated from the Pacoima Dam accelerograms should be made with caution.

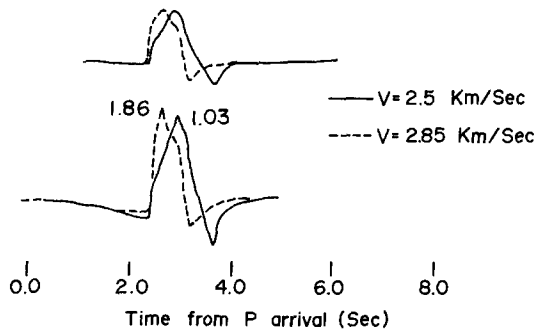


FIG. 12. Comparison of wave forms from the lower fault segment with rupture velocity as a parameter. The dashed and solid curves are not drawn to the same scale.

maximum surface velocities of 1.0 and 0.6 m/sec, respectively, for a rise time of 0.6 sec. Another example is contained in Figure 12, where wave forms produced by the lower dislocation with rupture velocities of 2.5 and 2.85 km/sec are shown. Although the data are fit better by the solid curve ( $V = 2.5$  km/sec), the solid and dashed curves could probably be made equivalent by modifying the dislocation time function (e.g., a rise

time of 1.0 sec for the model with  $V = 2.85$  km/sec will lead to a better fit). The two models, in which all factors are the same except the rupture velocity, produce peak velocities of 1.9 and 1.0 m/sec, respectively. This is an example of the importance of Mach number, mentioned earlier in the discussion of Figure 7. The effect of an increased Mach number can sometimes be offset by using a longer rise time or a longer length of rupture. An example is shown in the right side of Figure 7, where the solid curves for  $M = 0.92$ , which correspond to faulting to the surface, can be compared with the curves for the fault which stopped at depth and propagated with a slower rupture velocity (dashed curve,  $M = 0.81$ ). Although the comparison is not perfect, the similarity shows the difficulty that can arise in fitting a model to data from one station if no other information is available. A final example of the uncertainty in amplitude is shown in Figure 13. Here, the

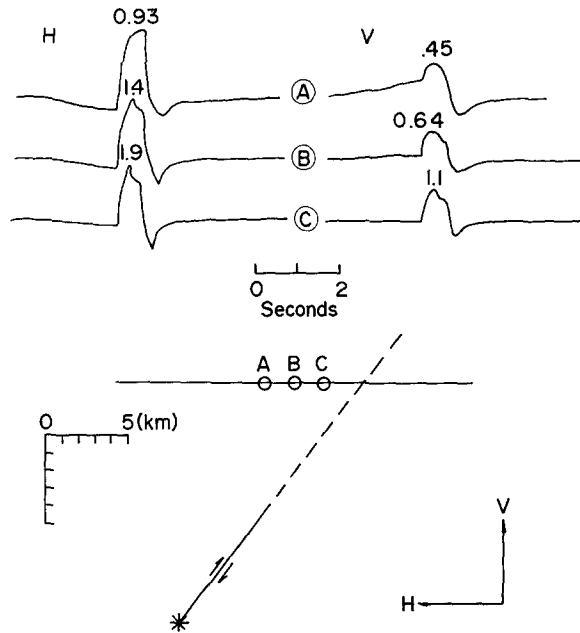


FIG. 13. Dependence of wave forms and amplitudes on location with respect to the fault surface. The rupture velocity was 2.85 km/sec. The ramp-like buildup before the  $S$  arrival on the  $V$  trace is caused by moving away from the node in the  $P$ -wave radiation pattern from the hypocenter. The curves for each spatial location have been independently scaled.

variation in amplitude is caused by the effect of the radiation pattern; the wave forms for three positions over a thrust fault are fairly similar, but the amplitudes of the peak motion on the horizontal component vary from 0.9 to 1.9 m/sec. If the geometry were not constrained by other data, this variation would obviously lead to uncertainties in the slip on the fault plane.

In spite of these uncertainties, it may be valuable to estimate the slip on the fault to see if it is consistent with the slip obtained by other investigators. A lower bound on the slip on the fault surface implied by the models can be obtained by scaling the calculated wave forms to the data. This will be a lower bound since the wave motion in this two-dimensional idealization will show less geometric attenuation than for an equivalent three-dimensional model (see Boore and Zoback, 1974). Of the models considered in this paper, the one used for the *upper part* of Figure 9 is the best fit to the data; taken at face value, it implies a slip on the fault plane of about 1 m. It is possible, however, to obtain a more realistic estimate by making an approximate correction for the difference in geometrical spreading. Such a correction can be obtained by comparison of two-

and three-dimensional models, as discussed in Boore and Zoback (1974). Unfortunately, for the station-fault geometry of interest, the comparison seems to be quite sensitive to small changes in location of the station with respect to the fault. The actual motion on the fault plane could be at least two to more than seven times the motion inferred from the two-dimensional model. This would put the inferred slip along the lower part of the fault surface into the range found by other investigators [less than 1 m by Mikumo (1973) to over 10 m by Trifunac (1974); Hanks (1974) and Alewine and Jordan (1973) find slips between 4 and 9 m and close to 4 m, respectively]. The strongest statement that can be made from the method used in this paper is that, if the model used in the *upper part* of Figure 9 is correct, the total dislocation was at least 2 m on the lower part of the fault surface. If the rise time of 0.6 is correct, this implies a dislocation velocity of 1.7 m/sec (where we assume the total dislocation is distributed equally on both sides of the slip surface). We can use this estimate of dislocation velocity to compute the minimum effective stress operating in the region of initial rupture by using the relation

$$\sigma = \mu \frac{(\dot{U})}{\beta} \max$$

(Housner, 1965; Ambraseys, 1969; Brune, 1970). With  $\mu = 3 \times 10^{11}$  dynes/cm<sup>2</sup> and  $\beta = 3.1$  km/sec, this gives a lower estimate of 165 bars for the effective stress.

Although the two-dimensional model could not be used to infer the amplitude of fault slip with any precision, it has been useful in testing various models of the rupturing process and suggests that the major pulse on the particle velocity traces comes from upward rupture starting around 13 km on a fault plane dipping at least 52°. A rupture velocity of 2.5 km/sec and a rise time of 0.6 sec are consistent with the data. It is obvious that more information on the faulting process is available in the data, but this information must be extracted by more sophisticated models than those employed here. It is particularly significant, however, that the simple model we have found is consistent with other data and reproduces the major features of the velocity wave form. This leads to more confidence in using the Pacoima Dam strong-motion records as a basis for design in earthquake engineering.

#### ACKNOWLEDGMENTS

We wish to thank Dr. Tom Hanks for several interesting discussions and valuable suggestions for the improvement of the manuscript.

This work was supported partly by the Division of Reactor Development and Technology, U.S. Atomic Energy Commission, and partly by National Science Foundation Grant GA-36135X.

#### REFERENCES

- Alewine, R. W. III and T. H. Jordan (1973). Generalized inversion of earthquake static displacement fields, *Geophys. J.* (in press).
- Allen, C. R., G. R. Engen, T. C. Hanks, J. M. Nordquist, and W. R. Thatcher (1971). Main shock and larger aftershocks of the San Fernando earthquake, February 9 through March 1, 1971, *U.S. Geol. Surv. Profess. Paper* 733, 17-20.
- Allen, C. R., T. C. Hanks, and J. H. Whitcomb (1973). San Fernando earthquake: seismological studies and their tectonic implications, *Calif. Div. Mines Geol., Bull.* 196, (in press.)
- Ambraseys, N. N. (1969). Maximum intensity of ground movements caused by faulting, *Proc. World Conf. Earthquake Engineering, 3rd, Santiago* 1, 154-171.
- Birch, F. (1966). Compressibility; elastic constants, Section 7 in *Handbook of Physical Constants*, S. P. Clark, Jr., Editor, *Geol. Soc. Am. Mem.* 97.

- Bolt, B. A. (1972). San Fernando rupture mechanism and the Pacoima Dam strong-motion record, *Bull. Seism. Soc. Am.* **62**, 1039–1045.
- Boore, D. M. (1973). The effect of simple topography on seismic waves: Implications for the accelerations recorded at Pacoima Dam, San Fernando Valley, California, *Bull. Seism. Soc. Am.* **63**, 1603–1609.
- Boore, D. M. and M. D. Zoback (1974). Near-field motions from kinematic models of propagating faults, *Bull. Seism. Soc. Am.* **64**, 321–342.
- Brune, J. N. (1970). Tectonic stress and the spectra of seismic shear waves, *J. Geophys. Res.* **75**, 4997–5009.
- Canitez, N. and M. N. Toksöz (1972). Static and dynamic study of earthquake source mechanism: San Fernando earthquake, *J. Geophys. Res.* **77**, 2583–2594.
- Christensen, N. I. (1966). Shear-wave velocities in metamorphic rocks at pressures to 10 kilobars, *J. Geophys. Res.* **71**, 3549–3556.
- Dillinger, W. and A. F. Espinosa (1971). Preliminary fault-plane solution for the San Fernando earthquake, *U.S. Geol. Surv. Profess. Paper 733*, 142–149.
- Hanks, T. C. (1974). The faulting mechanism of the San Fernando earthquake, submitted to *J. Geophys. Res.* (in press).
- Housner, G. W. (1965). Intensity of earthquake ground shaking near the causative fault. *Proc. World Conf. Earthquake Eng. 3rd*, Santiago, **1**, 94–109.
- Kamb, B., L. T. Silver, M. J. Abrams, B. A. Carter, T. H. Jordan, and J. B. Minster (1971). Pattern of faulting and nature of fault movement in the San Fernando earthquake, *U.S. Geol. Surv. Profess. Paper 733*, 41–54.
- Mikumo, T. (1973). Faulting process of the San Fernando earthquake of February 9, 1971 inferred from static and dynamic near-field displacements, *Bull. Seism. Soc. Am.* **63**, 249–269.
- Trifunac, M. D. (1974). A three-dimensional dislocation model for the San Fernando, California earthquake of February 9, 1971, *Bull. Seism. Soc. Am.* **64**, 149–172.
- Trifunac, M. D. and J. N. Brune (1970). Complexity of energy release during the Imperial Valley, California, earthquake of 1940, *Bull. Seism. Soc. Am.* **60**, 137–160.
- Trifunac, M. D. and D. E. Hudson (1971). Analysis of the Pacoima Dam accelerogram—San Fernando, California, earthquake of 1971, *Bull. Seism. Soc. Am.* **61**, 1393–1411.
- Tsai, T. B. and H. J. Patton (1972). Near-field small earthquakes—dislocation motion, *Semi-Annual Report 1*, Texas Instr. Inc. (prep. for Air Force Off. Seism. Res., Contract F44620-72-C-0073).
- U.S. Geological Survey Staff (1971). Surface faulting, *U.S. Geol. Surv. Profess. Paper 733*, 55–76.
- Wesson, R. L., W. H. K. Lee, and J. F. Gibbs (1971). Aftershocks of the earthquake, *U.S. Geol. Surv. Profess. Paper 733*, 22–29.
- Whitcomb, J. H. (1971). Fault-plane solutions of the February 9, 1971, San Fernando earthquake and some aftershocks, *U.S. Geol. Surv. Profess. Paper 733*, 30–32.
- Wyss, M. and J. N. Brune (1967). The Alaska earthquake of 28 March 1964; a complex multiple rupture, *Bull. Seism. Soc. Am.* **57**, 1917–1923.

U.S. GEOLOGICAL SURVEY  
345 MIDDLEFIELD ROAD  
MENLO PARK, CALIFORNIA 94025 (D.M.B.)

DEPT. OF GEOPHYSICS  
STANFORD UNIVERSITY  
STANFORD, CALIFORNIA 94305 (D.M.B. and M.D.Z.)

Manuscript received October 5, 1973.